Some aspects of AFM nanomechanical probing of surface polymer films

Hennady Shulha [a], Alexander Kovalev [b], Nikolai Myshkin [b], Vladimir V. Tsukruk [a,*]

[a] *Department of Materials Science and Engineering, Iowa State University, Ames, IA 50011, USA*
[b] *Metal–Polymer Institute, National Academy of Sciences, Gomel 246050, Belarus*

Abstract

We analyzed how the approach developed for the microindentation of non-uniform elastic solids can be adapted to analyze the atomic force microscopy (AFM) probing of ultrathin (1–100 nm thick) polymer films on a solid substrate, as well as polymer films with a multilayered structure. We suggested that recent Johnson's modification of the contact mechanics model that included a viscoelastic contribution could also be utilized to analyze rate-dependent loading data for polymer surfaces. The graded model proposed for microindentation experiments was modified allowing to account not only for variable elastic moduli within different layers but also for the gradient of properties between layers within a transition zone. Two examples of a recent application of this model for molecularly thick hyperbranched polymer monolayers (<3 nm thick) and tri-layered polymer films (20–40 nm thick) tethered to a solid substrate were presented and discussed. In both cases, complex shapes of both loading curves and elastic modulus depth profiles obtained from experimental AFM data were successfully fitted by the graded model with realistic structural parameters.
© 2004 Elsevier Ltd. All rights reserved.

Keywords: Nanomechanical probing; Elastic moduli; Polymer surface layers; Viscoelastic nanoscale properties

1. Introduction

Probing of the surface mechanical properties with nanometer-scale lateral and vertical resolution became a reality upon introduction of nanomechanical probing based on atomic force microscopy principles (AFM) [1,2]. Despite numerous technical issues associated with this AFM probing (e.g., non-axial loading, jump-into contact, nanoscale contact area, high local pressure, and topographical contributions), a number of successful applications of this approach have been demonstrated to date [3–5]. Recent applications to polymeric materials included nanomechanical probing of polymer hydrogels, thin polymer films, fiber-reinforced composites, organic lubricants, self-assembled monolayers, polymer blends, block-copolymers, polymer brushes, individual macro-molecules, and biological materials [6–10]. Absolute values of the elastic modulus were measured in the range from 0.001 to 30 GPa and in a wide range of temperatures and frequencies, for organic films with thickness down to 2 nm, and with vertical and lateral resolution as low as 1–2 and 5–10 nm, respectively. Elastic moduli (loss and storage), surface glass transition temperatures, and relaxation times all have been obtained with reasonable confidence by applying direct force–distance measurements and/or cantilever modulated (vertically as well as laterally) modes [11–13].

Spatial resolution unachievable by any other probing technique makes AFM nanomechanical probing a unique experimental tool. We believe that a further expansion of the AFM-based probing of ultrathin

---
* Corresponding author. Tel.: +1-515-294-6904; fax: +1-515-294-7202.

E-mail address: vladimir@iastate.edu (V.V. Tsukruk).

(below 10 nm) polymer films in the contact mode will rely on solving several fundamental issues: sophisticated evaluation of a substrate role in elastic response, the depth profiling of the elastic properties for multilayered and non-uniform films, and the evaluation of the rate-dependent contribution caused by the viscoelastic nature of polymeric materials (especially in the vicinity of the glass transition). In the present publication, we briefly discuss recent developments from our laboratory and recent results of corresponding research directly related to these topics.

2. Background: pure elastic response

The derivation of the elastic modulus from the AFM cantilever deflection data can be conducted by using a two-spring model of the interacting cantilever and the elastic surface (Fig. 1). The resulting indentation (penetration) depth is a function of the applied force (normal load) P, tip geometry (radius R or parabolic focus distance c), and the mechanical and adhesion properties of the contacting bodies. The normal load is calculated as $P = k_n \cdot z_{defl}$, where k_n is the vertical spring constant of the cantilever. The R (or c) and k_n are initial parameters, which must be calibrated before analysis. The Poisson's ratio, v, is a material parameter assumed to be known.

It has been shown that the general relationship between indentation depth, h, and normal load P can be presented in the form [14,15]:
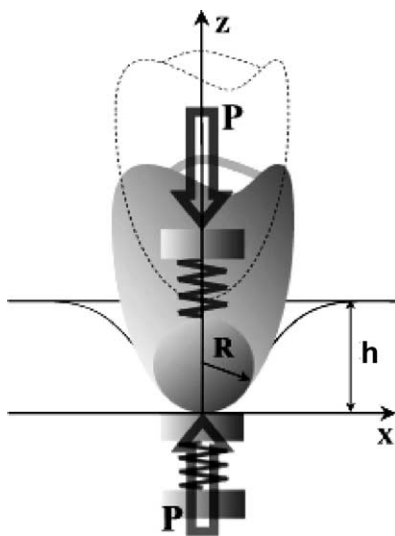
$$P = ah^b \tag{1}$$

Fig. 1. A two-spring model used to describe tip–surface interactions.

where a and b are specific model parameters (e.g., $b = 3/2$ for both Hertzian and parabolic Sneddon's contacts) [16].

The analysis of the indentation data and the calculation of Young's modulus can be conducted with the Sneddon formula [17]. The Sneddon model gives the relationship between surface stiffness, dP/dh and Young's modulus, E', in the form:

$$\frac{dP}{dh} = \frac{2\sqrt{A}}{\sqrt{\pi}} E' \tag{2}$$

where E' is the composite modulus defined as follows:

$$\frac{1}{E'} = \frac{1 - v_1^2}{E_1} + \frac{1 - v_2^2}{E_2} \tag{3}$$

E_1 and E_2 are elastic moduli of surface and an indentor (tip).

From dP/dh dependence and the contact area variation for a specific shape of the indentor (circular, pyramidal, and parabolic) one can evaluate the absolute value of the elastic modulus from Eq. (2). For a routine estimation of the elastic modulus for small indentation depth, the Hertzian model of a sphere-plane contact is routinely applied. For larger indentations, the Sneddon model with parabolic tip and a plane surface contact is successfully used. The Sneddon's equation gives results similar to the Hertzian equation but does not contain maximum indentation depth limitation and, thus, is usually used in our research.

The general Sneddon's equation can be converted to an appropriate numerical form applicable for AFM data processing as was discussed earlier [18]. For the parabolic indentor shape (best approximation for the AFM tip end) it gives an expression for the calculation of the *current* value of elastic modulus for a given indentation depth (non-uniform modulus distribution):

$$E_i = \frac{1}{2\sqrt{R}\beta}(1 - v^2)k_n \frac{\Delta z_{defl,i,i-1}}{\sqrt{h}\Delta h_{i,i-1}} \tag{4}$$

where $\beta = A_{cros}/A$, A_{cros} is cross-sectional indentor area at indentation depth h from the apex, β is equal to 2 for elastic deformation; and i, $i - 1$ refers to adjacent indentor (tip) displacements. This and other similar equations were used in our recent studies utilizing AFM probing of a variety of polymer surfaces [9,12,17,19,20].

Two major contributions cause significant deviations from pure elastic contact mechanical behavior (Fig. 2). First, a viscoelastic phenomenon results in additional viscous contribution causing "positive" deviations of the loading curves from the expected Hertzian behavior for purely elastic solids. Second, the presence of a stiff substrate beneath a very thin polymer film contributes in a limited film deformation under a high load resulting in "negative" deviations from pure elastic behavior
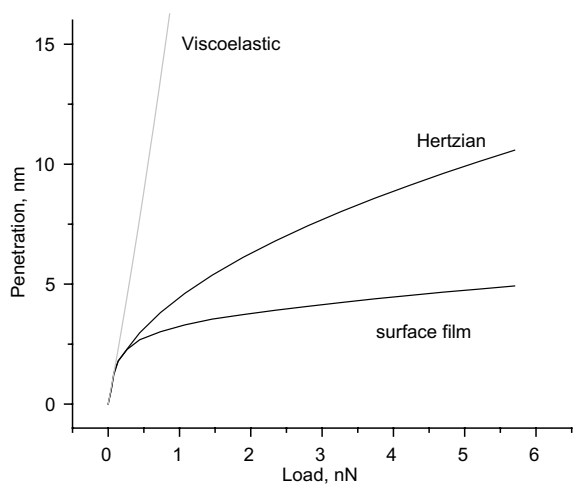
Fig. 2. Schematics of the deviation of the loading behavior from the Hertzian model due to the viscoelastic contribution and to the presence of a stiff substrate.

(Fig. 2). These two major complications can be treated as discussed below.

3. Rate-dependent response

The loading behavior (indentation depth versus normal load variation) of a wide range of polymer composites in glassy or rubbery states within limits of the elastic deformation can be reasonably well described with the Hertzian model (Fig. 3). Corresponding fits produced absolute values of the elastic modulus close to that expected for the bulk materials as demonstrated in Fig. 3 for several epoxy-based polymer composites as described in detail elsewhere [21]. However, a Hertzian fit was not satisfactory for a compliant film fabricated from a tri-block copolymer in the viscoelastic state (Fig. 3).

To analyze this rate-dependent behavior for the viscoelastic materials, we followed a Johnson's suggestion for the relationship between the contact area, a, load, P, and loading time, t, for viscoelastic solids in the form [22]:

$$a^3(\tau) = \frac{3RUT}{4E_\infty^*}[\tau - (1-k)(1-\exp(-\tau))] \tag{5}$$

where $\tau = t/T$ is the reduced time, $k = E_\infty^*/E_0^*$ is the reduced modulus with E_0^* being the initial, instantaneous modulus, and E_∞^* is the "equilibrium" relaxed modulus for an infinitely slow load, $U = P/t$ is the rate of loading, and T is the relaxation time of material.

This relationship was derived for a three-parameter linear viscoelastic model [22]. By varying two primary variables, E_0 and T, fitting the experimental data obtained at different rates can be conducted. It is worth to
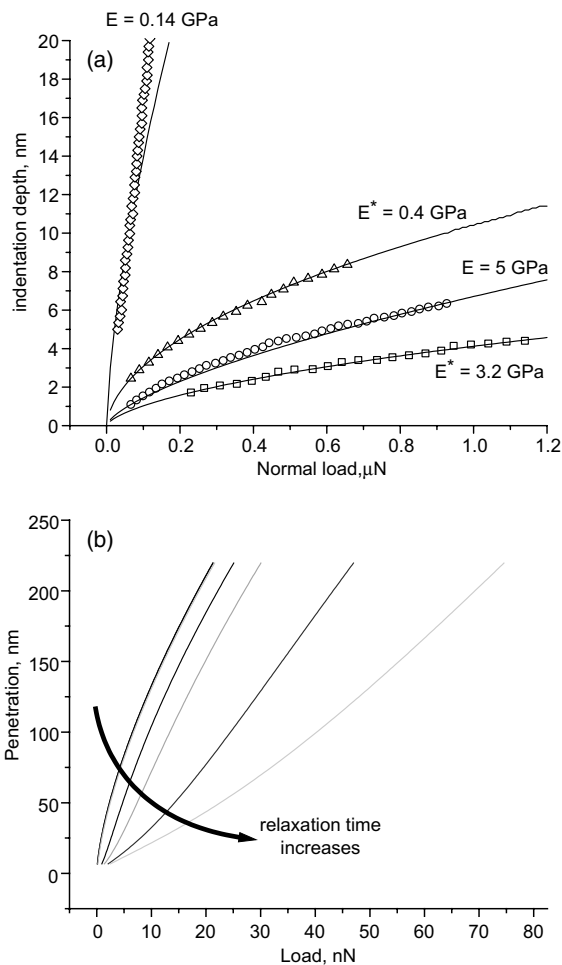

Fig. 3. (a) Examples of the fitting of the experimental data for a set of epoxy-based composite materials and the tri-block copolymer viscoelastic film ($E = 0.14$ GPa) with the Hertzian model (for experimental detail see Ref. [21]). (b) Theoretical calculation of the shape of the loading curves for a polymer surface with a variable relaxation time as estimated from Eq. (5).

note that the presence of the viscous contribution component can principally change the shape of the loading curve from the usual convex to concave as demonstrated for a series of model situations for a material with a variable relaxation time (Fig. 3). In fact, such concave curves have been observed for the viscoelastic materials in AFM experiments [18,21,23].

4. Substrate influence and multilayered surface structures

Several contact mechanics models have considered the role of concurrent deformation of a thin surface layer and an underlying substrate having very different

elastic moduli [24–26]. These models considered a different level of adhesion between films and substrates, suggested modified Hertzian equations, and demonstrated how the loading curves could be affected. However, these models have severe limitations related to both poorly defined interlayer interaction conditions and unstable solutions. In addition, these models considered only two-layered cases (film + substrate or bi-layered films).

A different approach was proposed by Doerner and Nix for analyzing the elastic recovery of solid thin films from microindentation experiments [27,28]. This approach was based on the representation of the depth-dependent compliance of two-layered elastic solids (e.g., film-substrate) as a linear combination of corresponding compliances weighted with a "transition function" reflecting a level of mutual influence of the two constituents (compare with the definition of the composite elastic modulus from Eq. (3)):

$$\frac{1}{E} = \frac{1}{E_f} \cdot (1 - e^{\alpha \cdot t/h}) + \frac{1}{E_s} \cdot (e^{\alpha \cdot t/h}) \qquad (6)$$

where E_f and E_s are the elastic moduli of the film and the substrate, h is the thickness of the film, t is the indentation depth, and α is the transition parameter responsible for mutual influence of substrate and film deformations. This approach was applied to the analysis of the microindentation data and produced consistent results for the elastic modulus and its depth profile of thin hard coatings with the thickness down to 10 nm [29–32].

In our efforts to adapt this approach to analyze the loading curves obtained from AFM force–distance data, we used Sneddon's or Hertzian equations (3) and (4). Then, we added an additional step in the fitting proce-

dure assuming that at any given indentation depth the elastic modulus value calculated from (4) is not a constant value but a variable represented by the Nix equation (6). Overall depth profile $E(h)$ and/or corresponding loading curve were used for fitting to find model parameters with the best thickness of the transition zone. The fitting procedure used a variable value of the elastic moduli of the film and the transition parameter α with the substrate elastic modulus usually kept to its bulk value. The transition parameter is empirically determined for each specific case.

To clarify the meaning of this parameter, we represented Eq. (6) in a different form as will be elaborated in great detail elsewhere [33]:

Fig. 5. The influence of the transition parameter α on the overall shape of the depth distribution curve of the elastic moduli. (a) A two layer model with a variable transition zone (α is 10^{-3}, 5×10^{-5}, 10^{-5}, 5×10^{-6}, 10^{-6}). (b) A tri-layer model with a variable transition zone. The decreasing of the value of α parameter results in the increasing of the transition zone and the smearing of the depth profile (α is selected equal for both layers and is 10^{-4}, 5×10^{-5}, 10^{-5}, 5×10^{-6}, 10^{-6}).
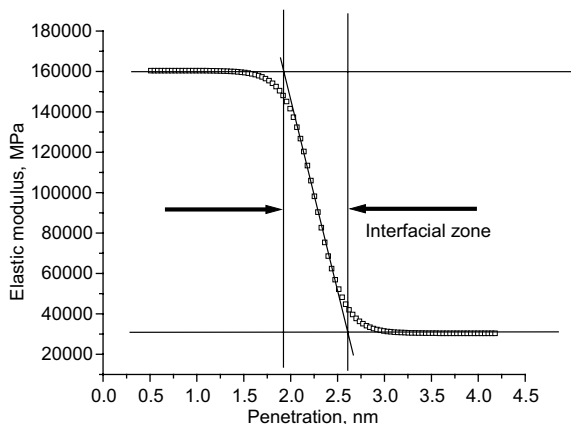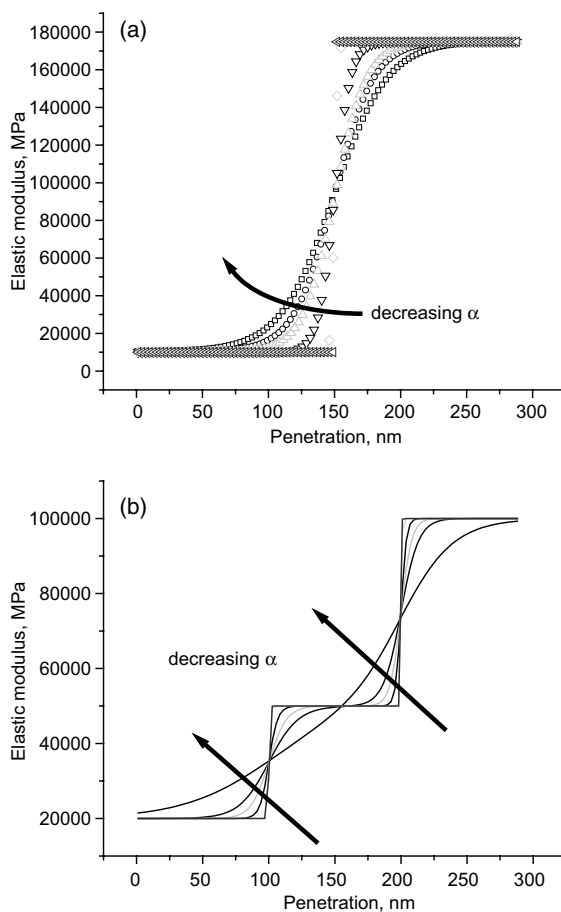

Fig. 4. The visualization of the depth profile for the surface with two different levels of the elastic modulus and the extensive interfacial zone (α is 10^{-4}, here and for other illustrative examples the values of the elastic modulus are arbitrary).

$$E' = \frac{E_1 - E_0}{1 + \exp(-a(E_1 - E_0)(z - z_0))} \tag{7}$$

This representation derived independently "visualizes" the depth profile for the interface with two different levels of the elastic moduli (Fig. 4). In this representation, two different levels of the elastic moduli are separated by the interfacial zone with the thickness controlled by the transition parameter α. High α-value corresponds to a sharp interface with virtually no gradient of the elastic modulus between two layers. Decreasing the value of the transition parameter results in a gradual increase of the transition zone with a broadening gradient expanding over larger and larger depth (increasing distances) (Fig. 5). Moreover, Eq. (7) can be expanded to include more complicated graded surface profiles such as a tri-layer profile presented in Fig. 5 as will be discussed elsewhere [33]. Through the variation of the two transition parameters and the values of the elastic moduli, different complex functions of non-homogeneous depth profiles can be generated. One such example is demonstrated by converting an initial tri-step function with sharp boundaries to a completely gradual, rising function (Fig. 5).

5. Selected examples of polymer surface layers

Experimental data in the form of force–volume mode for surface areas of 1×1 μm with 32×32 or 64×64 data points were obtained on Dimension 3000 and Multimode Nanoscope IIIa microscopes (Digital Instruments) according to a usual procedure adapted in our lab [34,35]. Spring constants were measured independently with added-mass technique and selected to be in the range from 0.05 to 5 N/m depending on sample elasticity and according to the criteria suggested earlier [36,37]. A number of force–distance curves (at least 15–20) was selected from an experimental array to represent typical shapes found in an overall surface histograms and for further analysis. These selected curves were averaged, smoothed, and used for the calculation of the depth profile and for the fitting procedure as described above. Here, we briefly present two selected examples of probing of ultrathin polymer films with detailed description of sample preparation and data collection.

5.1. Monolayers from dendritic molecules

Dendritic molecules studied here are represented by a hyperbranched polyesters of a third generation with hydroxyl terminal groups. The molecules were adsorbed on a functionalized silicon wafer surface to form a monolayered surface structure with thickness close to 3 nm and tethered to the solid substrate as described in detail elsewhere [38,39]. Original force–distance curves

showed non-monotonic shape, which is a characteristic of a compliant layer located on a stiff substrate (Fig. 6). In fact, the loading curve for this monolayer showed significant deviations from conventional Hertzian behavior for the layer deformation beyond 2 nm (Fig. 6).

However, the shape of the loading curves can be readily reproduced by using the multilayered model discussed above (Fig. 6). The two-layer model also describes the elastic modulus depth profile showing increasing absolute value for the larger deformation (Fig. 7). An overall profile obtained by the fitting procedure reveals the graded shape with a very thin (2.5 nm) compliant layer with the elastic modulus of 30–80 MPa
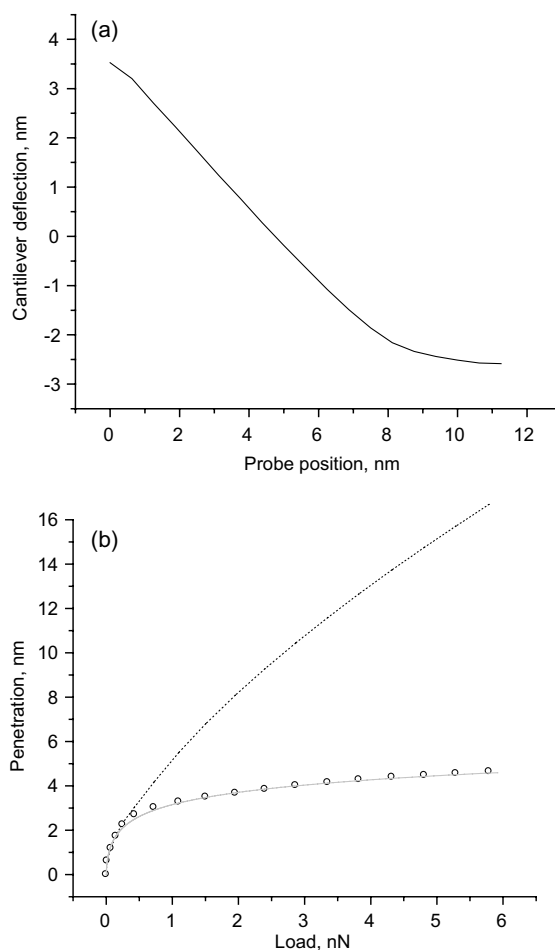

Fig. 6. (a) A typical force–distance curve obtained for the molecular monolayer from hyperbranched molecules. Initial part with a low slope (right bottom) corresponds to the monolayer deformation. Zero deflection corresponds to initial undisturbed state. (b) The fitting of the experimental data (empty circles) by the two-layer model (solid line) and Hertzian model (dot line) drawn for the same value of the elastic modulus.
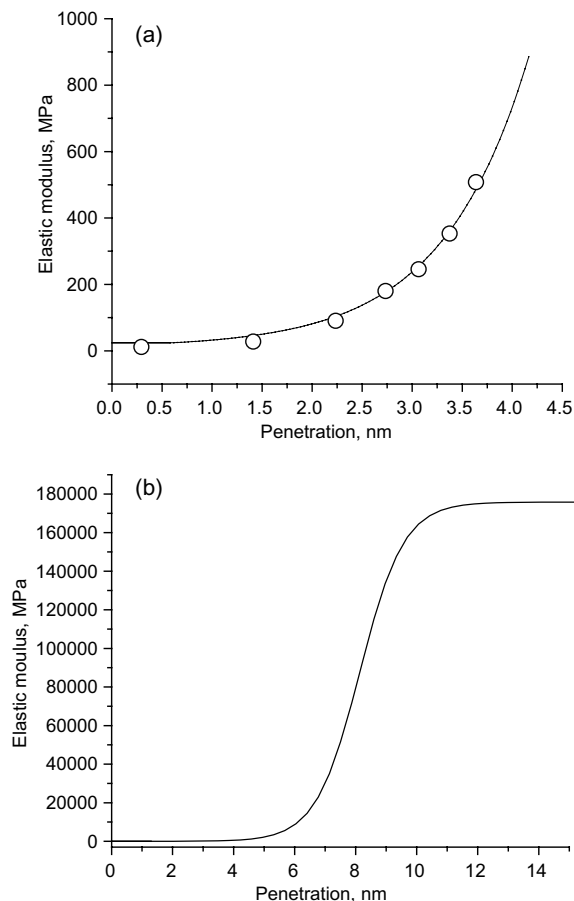
Fig. 7. (a) The fitting of the experimental data on the depth distribution of the elastic modulus (open circles) by the two-layer model (solid line). (b) Full depth distribution of the elastic modulus with the interfacial zone used for the best fitting procedure.

and the transition zone of 3 nm between the polymer monolayer and the silicon substrate as represented in the refined model (Fig. 7). These values correspond to structural parameters expected for polyester hyper-branched molecules tethered to the silicon oxide surface through epoxy-terminated self-assembled monolayer [38].

5.2. Tri-layer hard-soft-hard polymer film

"Triplex" polymer coatings, recently fabricated in our lab, represent a more complex case of a non-uniform elastic response distribution along the surface normal [40]. In this coating, a rubbery interlayer composed of a tri-block copolymer (poly[styrene-b-(ethylene-co-butyl-ene)-b-styrene]) was chemically tethered to the epoxy-functionalized silicon substrate and capped with a hard
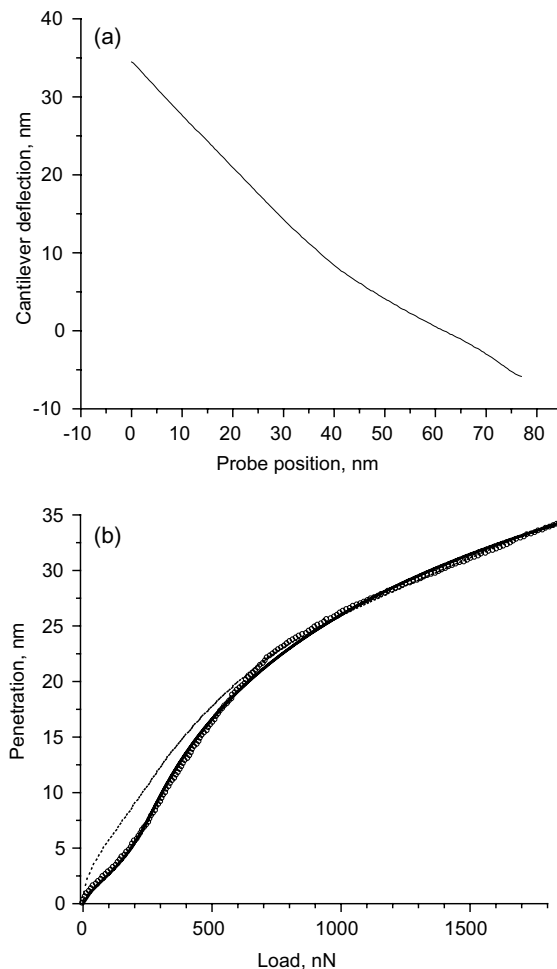

Fig. 8. (a) A force–distance curve for the tri-layer polymer coating [40]. (b) The fitting of the experimental data (empty circles) by the tri-layer model (solid line, almost completely masked by experimental data points) and an example of unsuccessful attempt to fit the data with Hertzian model (dot line).

layer of UV-polymerized polymethyl methacrylate [41]. The thickness of the compliant central interlayer was 8–10 nm and the thickness of the topmost layer was in the range of 5–30 nm. It has been demonstrated that the AFM probing could resolve three different deforma-tional regimes caused by a consequential deformation of different polymer layers [42].

Indeed, initial inspection of the force–distance curves revealed their highly non-monotonic character (Fig. 8). The corresponding loading curve displayed the S-shaped behavior far from being close to conventional mono-tonic Hertzian response (Fig. 8). However, the refining of the parameters of the tri-layered model constructed for these films produced excellent fitting of the complete loading curve with the complex shape (Fig. 8). On the
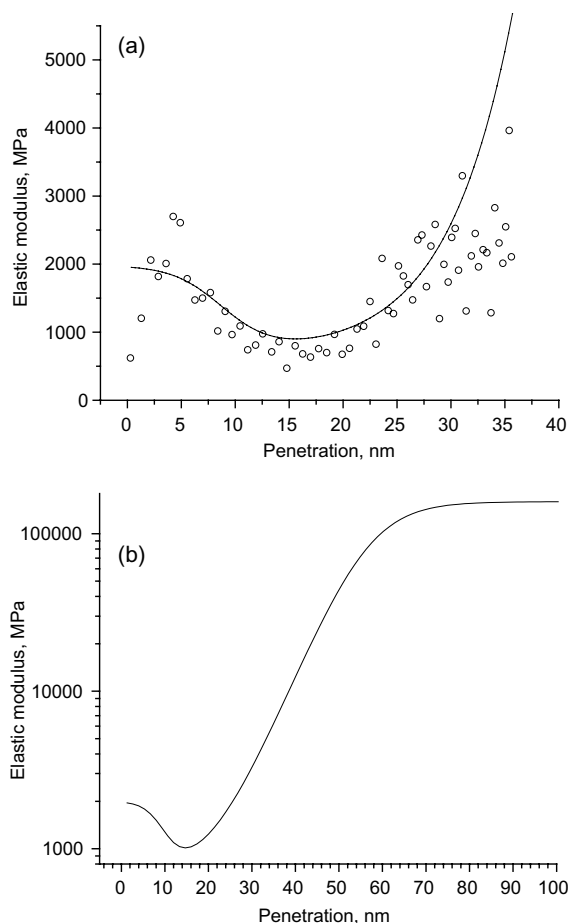
Fig. 9. (a) The fitting of the experimental depth distribution of the elastic modulus (empty circles) by the tri-layer model (filled squares). (b) Corresponding full depth distribution of the elastic modulus (pay attention to a logarithmic vertical scale to accommodate large difference in elastic moduli between the film and the substrate).

other hand, the depth profile of the elastic modulus clearly showed three different regions with higher and lower apparent elastic moduli (Fig. 9). The best fit has been achieved with the tri-layer model composed of the topmost hard layer of 5 nm thick with the elastic modulus of 2000 MPa, a central interlayer of 20 nm thick and the apparent elastic modulus of 800 MPa, and the solid substrate with the elastic modulus of 160 GPa (Fig. 9). The thickness of the transition zone did not exceed 20 nm that indicates a gradient boundary between polymer layers in this tri-layer nanocoating.

6. Conclusions

In conclusion, we demonstrated that the approach developed for the microindentation of non-uniform elastic solids can be adapted to analyze the AFM probing of ultrathin (tens of nanometers) polymer films on solid substrates and polymer films with the vertically layered structure. This graded model allows to account not only for the variable elastic modulus within different layers, but also for the different gradient of the elastic properties between adjacent layers described by the transition zone parameter. Two examples of the applications of the approach proposed for the molecularly thick hyperbranched polymer monolayer and the tri-layer polymer film tethered to the solid substrate have been presented and discussed. In both cases, the complex shape of the experimental loading curves and the elastic modulus depth profiles were successfully simulated using the graded models with realistic structural parameters.

References

[1] Domke J, Radmacher M. Measuring the elastic properties of thin polymer films with the atomic force microscope. Langmuir 1998;14:3320.

[2] Chen X, Vlassak JJ. Numerical study on the measurement of thin film mechanical properties by means of nano-indentation. J Mater Res 2001;16:2974.

[3] Persson B. Sliding friction. Surf Sci Rep 1999;33:83.

[4] Vanlandingham MR, McKnight SH, Palmese GR, Ellings JR, Huang X, Bogetti TA, et al. Nanoscale indentation of polymer systems using the atomic force microscope. J Adhesion 1997;64:31.

[5] Overney RM. Nanotribological studies on polymers. Trends Polym Sci 1995;3:359.

[6] Kurokawa T, Gong JP, Osada Y. Substrate effect on topographical, elastic, and frictional properties of hydrogels. Macromolecules 2002;35:8161.

[7] Moon SH, Foster MD. Near surface nanomechanical behavior of pressure-sensitive adhesives using lateral modulation scanning probe microscopy. Langmuir 2002;18:1865.

[8] Lemoine P, Mc Laughlin J. Nanomechanical measurements on polymers using contact mode atomic force microscopy. Thin Solid Films 1999;339:258.

[9] Eaton P, Fernandez EF, Ewen RJ, Nevell TG, Smith JR, Tsibouklis J. Combined nanoindentation and adhesion force mapping using the atomic force microscope: investigations of a filled polysiloxane coating. Langmuir 2002; 18:10011.

[10] Gorbunov V, Fuchigami N, Stone M, Grace M, Tsukruk VV. Biological thermal detection: micromechanical and microthermal properties of biological infrared receptors. Biomacromolecules 2002;3:106.

[11] Du B, Tsui OKC, Zhang Q, He T. Study of elastic modulus and yield strength of polymer thin films using atomic force microscopy. Langmuir 2001;17:3286.

[12] Asif Syed SA, Wahl KJ, Colton RJ, Warren OL. Quantitative imaging of nanoscale mechanical properties using hybrid nanoindentation and force modulation. J Appl Phys 2001;90:1192.

[13] Tsukruk VV, Huang Z. Micro-thermomechanical properties of heterogeneous polymer films. Polymer 2000;41:5541.

[14] Oliver WC, Pharr GM. An improved technique for determining hardness and elastic modulus using load and displacement sensing indentation experiments. J Mater Res 1992;7:1564.

[15] Johnson KL, Kendall K, Roberts AD. Surface energy and the contact of elastic solids. Proc Roy Soc London A 1971;324:301.

[16] Pharr GM, Oliver WC, Brotzen FB. On the generality of the relationship among contact stiffness, contact area, and elastic modulus during indentation. J Mater Res 1992;7: 613.

[17] Johnson KL. Contact mechanics. Cambridge: Cambridge University Press; 1985.

[18] Chizhik SA, Huang Z, Gorbunov VV, Myshkin NK, Tsukruk VV. Micromechanical properties of elastic polymeric materials as probed by scanning force microscopy. Langmuir 1998;14:2606.

[19] Tsukruk VV, Huang Z, Chizhik SA, Gorbunov VV. Probing of micromechanical properties of compliant polymeric materials. J Mater Sci 1998;33:4905.

[20] Tsukruk VV, Sidorenko A, Gorbunov VV, Chizhik SA. Surface nanomechanical properties of polymer nanocomposite layers. Langmuir 2001;17:6715.

[21] Chizhik SA, Gorbunov VV, Fuchigami N, Luzinov I, Tsukruk VV. Surface force spectroscopy of elastomeric nanoscale films. Macromol Symp 2001;167:169.

[22] Johnson KL. Contact mechanics and adhesion of viscoelastic spheres. In: Tsukruk VV, Wahl K, editors. Microstructure and microtribology of polymer surfaces, ACS Symposium Series 741. USA: ACS; 1998. p. 24.

[23] Tsukruk VV, Gorbunov VV, Huang Z, Chizhik SA. Dynamic microprobing of viscoelastic polymer properties. Polym Int 2000;49:441.

[24] Suresh S. Graded materials for resistance to contact deformation and damage. Science 2001;292:2447.

[25] Makushkin AP. Deformation of compliant layer during the indentation of spherical indentor. Evaluation of contact pressure. Frict Wear 1990;11:423.

[26] Giannakopoulos AE, Suresh S. Indentation of solids with gradients in elastic properties: Part II. Axisymmetric indentors. Int J Solids Struct 1997;34(19):2393.

[27] Doerner MF, Nix WD. A method for interpreting the data from depth-sensing indentation instruments. J Mater Res 1986;1:601.

[28] Saha R, Nix WD. Effects of the substrate on the determination of thin film mechanical properties by nanoindentation. Acta Mater 2002;50:23.

[29] Mencik J, Munz D, Quandt E, Weppelmann ER. Determination of elastic modulus of thin layers using nanoindentation. J Mater Res 1997;12:9.

[30] Saha R, Nix WD. Soft films on hard substrates—nanoindentation of tungsten films on sapphire substrates. Mater Sci Eng A 2001;319:898.

[31] Sawa T, Akiyama Y, Shimamoto A, Tanaka K. Nanoindentation of a 10 nm thick thin film. J Mater Res 1999;14:2228.

[32] Gao H, Chiu CH, Lee J. Elastic contact versus indentation modeling of multi-layered materials. Int J Solids Struct 1992;29:2471.

[33] Shulha H, Kovalev A, Lemieux M, Myshkin N, Tsukruk VV. Influence of substrate on mechanical properties of multilayer polymer systems. J Mater Res, in press.

[34] Tsukruk VV, Gorbunov VV. Nanomechanical probing with scanning force microscopy. Microsc Today 2001;01-1:8.

[35] Tsukruk VV, Gorbunov VV. Nanomechanical analysis of polymer surfaces. Probe Microsc 2002;3–4:241.

[36] Hazel JL, Tsukruk VV. Spring constants of composite ceramic/gold cantilevers for scanning probe microscopy. Thin Solid Films 1999;339:249.

[37] Huang Z, Chizhik SA, Gorbunov VV, Myshkin NK, Tsukruk VV. Scanning force microscopy of micromechanical properties of polymers. In: Tsukruk VV, Wahl K, editors. Microstructure and microtribology of polymer surfaces, ACS Symposium Series 741. USA: ACS; 2001. p. 177.

[38] Shulha H, Zhai X, Tsukruk VV. Molecular stiffness of individual hyperbranched macromolecules at solid surfaces. Macromolecules 2003;36:2825.

[39] Tsukruk VV, Shulha H, Zhai X. Nanoscale stiffness of individual dendritic molecules and their aggregates. Appl Phys Lett 2003;82:907.

[40] Tsukruk VV, Sidorenko A, Yang H. Polymer nanocomposite coatings with non-linear elastic response. Polymer 2002;43:1695.

[41] Sidorenko A, Ahn HS, Kim D, Yang H, Tsukruk VV. Wear stability of polymer nanocomposite coatings with trilayer architecture. Wear 2002;252:946.

[42] Tsukruk VV, Ahn HS, Kim D, Sidorenko A. Triplex molecular layers with nonlinear nanomechanical response. Appl Phys Lett 2002;80:4825.